SCALE SIMILARITY REVISITED IN LES

Christer Fureby
Div. of Weapons and Protection, Warheads and Propulsion
The Swedish Defense Research Agency – FOI, SE 147 25, Tumba, Sweden
fureby@foi.se

Rickard Bensow, Tobias Persson
Dept. of Shipping and Marine Technology
Chalmers University of Technology, SE 412 96 Göteborg, Sweden
ribe@na.chalmers.se, tobias.persson@chalmers.se

ABSTRACT
A reformulation of the Large Eddy Simulation (LES) equations is presented, based on an alternative decomposition of the subgrid stress tensor leading to a modified Leonard term, which becomes an integral part of the LES equations. This formulation clearly emphasizes the difference between Reynolds Average Navier-Stokes (RANS) models and LES. The reformulated LES model is tested on several well-established flows, such as jet flows, channel flows and the flow past a circular cylinder and a prolate spheroid, and the results are compared with results from conventional LES and data. For the simpler cases at lower Re-number, the differences between the models are small, while on the more complicated cases at higher Re-number, the proposed model shows improved behaviour as compared to the conventional LES model.

INTRODUCTION
Large Eddy Simulation (LES) is based on the idea of separating scales, and separates the flow into two regimes by means of the convolution $\bar{f}(\mathbf{x},t)=G(\mathbf{x},\Delta)*f(\mathbf{x},t)$, where $G(\mathbf{x},\Delta)$ is the filter kernel of width Δ. The first regime, comprised of large scales that can be resolved on the grid, is computed using a space time accurate algorithm. The other regime, the small, unresolved, scales, ranges from the grid-scale cut-off down to the Kolmogorov scales. Applying the filtering procedure to the incompressible Navier-Stokes Equations (NSE) yields,

$$\partial_t(\bar{\mathbf{v}})+\nabla\cdot(\bar{\mathbf{v}}\otimes\bar{\mathbf{v}})=-\nabla\bar{p}+\nabla\cdot\bar{\mathbf{S}}-\nabla\cdot\mathbf{B}+\mathbf{m}^v,\ \nabla\cdot\bar{\mathbf{v}}=0 \qquad (1)$$

where $\mathbf{B}=\overline{\mathbf{v}\otimes\mathbf{v}}-\bar{\mathbf{v}}\otimes\bar{\mathbf{v}}$ is the subgrid stress tensor and $\mathbf{m}^v=[G*,\nabla](\mathbf{v}\otimes\mathbf{v}+p\mathbf{I}-\mathbf{S})$ the commutation error, where $[G*,\nabla]f=\nabla f-\nabla\bar{f}$, Sagaut (2001). Both $\nabla\cdot\mathbf{B}$ and $\mathbf{m}^v$ are subject to modeling, and are thus often combined. The direct computation of the large, energy containing eddies (being geometry and flow dependent) gives LES more generality than Reynolds Averaged Navier-Stokes (RANS) models, which model the full spectrum of turbulent motions. Subgrid modeling is necessary to close (1) and to include the effects of the small, unresolved, eddy scales.

Here, we derive a modified formulation of the LES equations which clearly emphasizes the difference between RANS and LES, and embodies primarily a re-definition of the components in **B** that results in less stringent modeling requirements. Moreover, a framework is proposed and tested for subgrid modeling in this new setting. Finally, results from the proposed LES approach are presented for jet flow at Re=95,000; fully developed turbulent channel flow at Re_τ=395, 595 and 1800; flow past a circular cylinder at Re=3900 and 140,000; and flow past a prolate spheroid at $\alpha=10°$ and 20° angle-of-attack at Re= $1.6\cdot10^6$. Improved agreement with reference data is found, primarily at the high Re number cases, suggesting that the proposed formulation better represents the energy redistribution between the resolved and unresolved scales.

MATHEMATICAL AND PHYSICAL CONSIDERATIONS
A prerequisite when developing models for **B** is that the model inherits all the essential mathematical and physical properties of **B**, cf. Fureby & Tabor (1997), Vreman *et al*, (1994) and Speziale (1985). The principle of frame indifference states that all physical laws which hold in a dynamic process are the same for any observer, i.e. in every frame of reference Σ. Hence, all well-posed LES models must have the same transformation properties as the unfiltered NSE under a change of frame $\Sigma\rightarrow\Sigma^*$, given by $\mathbf{x}^*(\mathbf{X},t)=\mathbf{c}(t)+\mathbf{Q}(t)\mathbf{x}(\mathbf{X},t)$ and $t^*=t$. Here, **X** is the material points occupying the body D, **c**(t) a translation and **Q**(t) a rotation. From $\bar{\mathbf{v}}(\mathbf{x},t)=G(\Delta)*\mathbf{v}(\mathbf{x},t)$, it follows that the filtering is frame indifferent if $G=G(|\mathbf{x}|,\Delta)$. By differentiating the change of frame and by using $\mathbf{v}(\mathbf{x},t)\equiv\dot{\mathbf{x}}(\mathbf{X}(\mathbf{x},t),t)$ it follows that the subgrid velocity fluctuations transform as $\mathbf{v}'^*=\mathbf{Q}\mathbf{v}'$ which further implies that $\mathbf{v}'$ is invariant under $\Sigma\rightarrow\Sigma^*$. From the chain rule of differentiation and the definition of the change of frame it follows that $\nabla^*=\mathbf{Q}\nabla$ and $\partial_{t^*}=\partial_t$, whereas the constitutive equations for a linear viscous fluid, $\bar{\mathbf{S}}=2\nu\bar{\mathbf{D}}$, transforms as $\bar{\mathbf{S}}^*=\mathbf{Q}\bar{\mathbf{S}}\mathbf{Q}^T$, since $\bar{\mathbf{D}}^*=\mathbf{Q}\bar{\mathbf{D}}\mathbf{Q}^T$. Hence, the LES equations (1) transform as the unfiltered NSE provided that $\mathbf{B}^*=\mathbf{Q}\mathbf{B}\mathbf{Q}^T$. When developing subgrid models for the subgrid stress tensor **B**, the model of the subgrid stress tensor should satisfy this constraint.

CLASSICAL DECOMPOSITION AND MODELING
By applying the decomposition $\mathbf{v}=\bar{\mathbf{v}}+\mathbf{v}'$ to the first term (i.e. the $\mathbf{v}\otimes\mathbf{v}$ term) in the definition of the subgrid stress tensor **B** this tensor can, following Sagaut (2001), be decomposed as follows,

$$\mathbf{B}=\left(\overline{\mathbf{v}\otimes\mathbf{v}}-\bar{\mathbf{v}}\otimes\bar{\mathbf{v}}\right)=\left(\overline{\bar{\mathbf{v}}\otimes\bar{\mathbf{v}}}-\bar{\mathbf{v}}\otimes\bar{\mathbf{v}}\right)+\left(\overline{\bar{\mathbf{v}}\otimes\mathbf{v}'}+\overline{\mathbf{v}'\otimes\bar{\mathbf{v}}}\right)+\left(\overline{\mathbf{v}'\otimes\mathbf{v}'}\right) \qquad (2)$$
$$=\mathbf{L}+\mathbf{C}+\mathbf{R}$$

where the different component stress tensors can be ascribed different physical meanings, Pope (2000). From (2) it is clear that $\mathbf{L}$ can be computed explicitly and thus reducing the modeling efforts to $\mathbf{C}$ and $\mathbf{R}$. However, by analyzing the transformation properties of $\mathbf{L}$, $\mathbf{C}$ and $\mathbf{R}$ under $\Sigma\rightarrow\Sigma^*$ it is clear that $\mathbf{L}$ and $\mathbf{C}$ are not individually frame indifferent, whereas $\mathbf{R}$ is. This implies that if $\mathbf{L}$ is explicitly evaluated, $\mathbf{C}$ and $\mathbf{R}$ must be modeled individually, with models recognizing their individual transformation properties. For $\mathbf{R}$ this is straightforward, since all subgrid viscosity models are frame indifferent (as $\overline{\mathbf{D}}^*=\mathbf{Q}\overline{\mathbf{D}}\mathbf{Q}^T$) but developing models for $\mathbf{C}$ that satisfies $\mathbf{C}^*=\mathbf{Q}\mathbf{C}\mathbf{Q}^T+\mathbf{Z}$, where $\mathbf{Z}=\overline{\mathbf{v}}'\otimes(\dot{\mathbf{c}}+\mathbf{Q}\dot{\mathbf{x}})+(\dot{\mathbf{c}}+\mathbf{Q}\dot{\mathbf{x}})\otimes\overline{\mathbf{v}}'$ results from the change of frame, is not easy. If this leads to neglecting $\mathbf{C}$ whilst retaining $\mathbf{L}$ and $\mathbf{R}$, $\mathbf{B}$ will have incorrect properties.

The classical subgrid models are the Smagorinsky model (SMG), Smagorinsky (1963), and the One Equation Eddy Viscosity Model (OEEVM), Schumann (1975), in which $\mathbf{B}=-2\nu_k\overline{\mathbf{D}}$, where ν_k is the subgrid viscosity. Close to walls Δ, is usually changed to $\Delta=\Delta(1-e^{-u_\tau y/A\nu})$ to accommodate a correct scaling of the subgrid stress compentents as the wall is approached. In order to better handle high Re-number wall bounded flows a subgrid wall model was proposed by Fureby *et al.* (2004) and Wikström *et al.* (2004), in which the subgrid viscosity ν_k in the first cell adjacent to the wall is evaluated to comply with the universally assumed law of the wall (hereafter denoted by WM). The assumption behind this model is that the streaks and ejection events are as frequent in wall-bounded flows as are vortices in free flows.

REFORMULATION OF THE LES MODEL

As a direct remedy to the individual component stress tensor modeling, we suggest that an alternative to the decomposition in (2) in which the decomposition $\mathbf{v}=\overline{\mathbf{v}}+\mathbf{v}'$ is applied to both terms in the definition of the subgrid stress tensor $\mathbf{B}$. Then, $\mathbf{B}$ can be decomposed as,

$$\begin{aligned}\mathbf{B}&=(\overline{\overline{\mathbf{v}}\otimes\overline{\mathbf{v}}}-\overline{\overline{\mathbf{v}}}\otimes\overline{\overline{\mathbf{v}}})+(\overline{\overline{\mathbf{v}}\otimes\mathbf{v}'}-\overline{\overline{\mathbf{v}}}\otimes\overline{\mathbf{v}'}+\overline{\mathbf{v}'\otimes\overline{\mathbf{v}}}-\overline{\mathbf{v}'}\otimes\overline{\overline{\mathbf{v}}})\\&+(\overline{\mathbf{v}'\otimes\mathbf{v}'}-\overline{\mathbf{v}'}\otimes\overline{\mathbf{v}'})=\tilde{\mathbf{L}}+\tilde{\mathbf{C}}+\tilde{\mathbf{R}}\end{aligned}\qquad(3)$$

where the different component stress tensors can be ascribed similar physical meanings as before, but with one significant difference; all three component stress tensors are now frame indifferent. A similar decomposition was suggested already in 1996 by Germano (1996), but on other grounds. This suggests that we should reformulate the LES equations in such a way that the modified Leonard term $\tilde{\mathbf{L}}$ becomes an explicit part of the LES equations and not of the subgrid stress tensor which, in turn, is redefined as the sum of the modified cross and Reynolds stress tensors,

$$\begin{aligned}&\partial_t(\overline{\mathbf{v}})+\nabla\cdot(\overline{\mathbf{v}}\otimes\overline{\mathbf{v}})=-\nabla\overline{p}+\nabla\cdot\overline{\mathbf{S}}-\nabla\cdot(\overline{\overline{\mathbf{v}}\otimes\overline{\mathbf{v}}}-\overline{\overline{\mathbf{v}}}\otimes\overline{\overline{\mathbf{v}}}-\tilde{\mathbf{B}})+\mathbf{m}^v\\&\tilde{\mathbf{B}}=\tilde{\mathbf{C}}+\tilde{\mathbf{R}}=(\overline{\overline{\mathbf{v}}\otimes\mathbf{v}'}-\overline{\overline{\mathbf{v}}}\otimes\overline{\mathbf{v}'}+\overline{\mathbf{v}'\otimes\overline{\mathbf{v}}}-\overline{\mathbf{v}'}\otimes\overline{\overline{\mathbf{v}}})+(\overline{\mathbf{v}'\otimes\mathbf{v}'}-\overline{\mathbf{v}'}\otimes\overline{\mathbf{v}'})\end{aligned}\qquad(4)$$

with $\nabla\cdot\overline{\mathbf{v}}=0$. In (4), the presence of the modified Leonard term $\tilde{\mathbf{L}}=(\overline{\overline{\mathbf{v}}\otimes\overline{\mathbf{v}}}-\overline{\overline{\mathbf{v}}}\otimes\overline{\overline{\mathbf{v}}})$ clearly distinguishes them from the RANS equations, emphasizing the importance of the smallest resolved scales. This explicit and exact term is identical to the scale similarity model, Bardina *et al.* (1980), found to have high correlation with DNS data. Closure modeling is thus only required for the modified cross- and Reynolds terms, $\tilde{\mathbf{C}}$ and $\tilde{\mathbf{R}}$ respectively, which now can be modeled separately or together.

SUBGRID CLOSURE MODELING OF B

Next we will discuss possible closure strategies for the modified subgrid stress tensor $\tilde{\mathbf{B}}$ and its component stress tensors $\tilde{\mathbf{C}}$ and $\tilde{\mathbf{R}}$, respectively. In the simplest approach $\tilde{\mathbf{B}}$ is modeled by a subgrid viscosity model,

$$\tilde{\mathbf{B}}=\tilde{\mathbf{C}}+\tilde{\mathbf{R}}=-2\nu_k\overline{\mathbf{D}}_D\qquad(5)$$

Alternatively this can be thought of as neglecting one of the components of $\tilde{\mathbf{B}}$. The resulting LES model, (i.e. (4) closed by (5)) is then identical to the conventional LES model (1) using the mixed model for closure of the subgrid stress tensor $\mathbf{B}$. Candidate subgrid models are the SMG model, (Smagorinsky (1963)), the OEEVM, (Schumann (1975)), or the Dynamic Smagorinsky (DSMG) model, (Germano *et al.* (1991)).

A more elaborate model for $\tilde{\mathbf{B}}$ is obtained if the original structure of $\tilde{\mathbf{B}}$ is retained such that $\tilde{\mathbf{C}}$ and $\tilde{\mathbf{R}}$ are modeled separately. Based on the physical processes represented by each of the components it is appropriate to model $\tilde{\mathbf{R}}$ by a subgrid viscosity model i.e. $\tilde{\mathbf{R}}=-2\nu_k\overline{\mathbf{D}}_D$, with ν_k being evaluated using any of the previous submodels. A more difficult modeling problem arises when considering $\tilde{\mathbf{C}}$ whose effects are less known. Instead of using functional models we attempt to close this term by using modern structural models as inspired by the ADM of Stolz *et al.* (2001). Following van-Cittert (1931), an approximation $\mathbf{v}^*$ to $\mathbf{v}$ can be computed by repeated filtering of $\overline{\mathbf{v}}$ such that $\mathbf{v}^*=G_N^{-1}*\overline{\mathbf{v}}\approx\sum_{k=0}^{N}(1-G)^k*\overline{\mathbf{v}}$ which in turn leads to an approximation $\mathbf{v}'^*$ to $\mathbf{v}'$ computed from $\mathbf{v}'^*=\mathbf{v}^*-\overline{\mathbf{v}}=G_N^{-1}*\overline{\mathbf{v}}-\overline{\mathbf{v}}\approx\sum_{k=1}^{N}(1-G)^k*\overline{\mathbf{v}}$. Following Stolz *et al.* (2001), this series expansion is truncated at N=5 resulting in $\mathbf{v}'^*\approx\mathbf{v}^*-\overline{\mathbf{v}}=(\overline{\mathbf{v}}-\overline{\overline{\mathbf{v}}})+(\overline{\mathbf{v}}-2\overline{\overline{\mathbf{v}}}+\overline{\overline{\mathbf{v}}})+\ldots$. Applying this approximation to the expression for the modified cross term $\tilde{\mathbf{C}}$ finally yields,

$$\tilde{\mathbf{B}}=\tilde{\mathbf{C}}+\tilde{\mathbf{R}}=\left(\overline{\overline{\mathbf{v}}\otimes\mathbf{v}'^*}-\overline{\overline{\mathbf{v}}}\otimes\overline{\mathbf{v}'^*}+\overline{\mathbf{v}'^*\otimes\overline{\mathbf{v}}}-\overline{\mathbf{v}'^*}\otimes\overline{\overline{\mathbf{v}}}\right)-2\nu_k\overline{\mathbf{D}}_D\qquad(6)$$

In the computations to be presented, the LES model (4)-(6) will be compared to the conventional LES model (1), using eddy viscosity models for the closure of ν_k.

NUMERICAL METHODS

A finite volume method for arbitrary cell-shapes and a segregated approach described by Weller *et al.* (1997), is used to discretize the LES equations. The space discretization uses high-order econstruction of the convective fluxes and central differencing of the inner derivatives of the viscous flux terms with compact 2nd order stencils and time integration is performed by explicit 2nd order backward differencing which thus guarantees overall 2nd order accuracy and low numerical diffusion. The pressure-velocity coupling is handled with a PISO procedure based on a modified Rhie & Chow interpolation for the cell-centered data storage structure. The equations are solved sequentially, with iteration over the explicit source terms, with a Courant number of CFL<0.3.

ROUND TURBULENT JET FLOWS

The first test case is that of a round turbulent jet. We consider a jet with Re_D=95,500, Hussein *et al.* (1994), based on the jet-exit velocity, v_J, diameter, D, and molecular viscosity, v, emerging into ambient air with a co-flow velocity of v_0. The velocity profile at the nozzle is assumed to be top-hat shaped with no superimposed perturbations, e.g. Hussein *et al.* (1994). The computational domain is cylindrical with a length of 60D and a diameter of 20D, and the grid consists of 240×50×100 cells in the axial, radial and tangential directions. The grid is refined in the jet-shear layers around the nozzle, and stretched in other regions of the flow. Conventional incompressible inflow and outflow boundary conditions are provided together with circumferential freestream boundary conditions.

Figures 1a and 1b shows axial profiles of the time-averaged axial velocity component $\langle \overline{v}_x \rangle$ and the corresponding rms-velocity fluctuations $v_x^{rms}=\langle(\overline{v}_x-\langle \overline{v}_x \rangle)^2\rangle^{1/2}$ respectively. Comparison is made with several experimental data sets, Crow & Champagne (1971), Lau *et al.* (1979) and Cohen & Wygnanski (1987). For the axial profiles of $\langle \overline{v}_x \rangle$ all LES models, both conventional and proposed, are in good agreement with data, e.g. the length of the potential core is ~4.5D. Concerning the rms-velocity fluctuations v_x^{rms} we find acceptable agreement between LES and experimental data, with peak values occurring towards the end of the mixing region. The proposed models, (4)-(6), are however generally in better agreement with data than the conventional LES model, in particular for x/D≤15. The reason for this is the improved prediction of the kinetic energy cascade rate of the proposed models.

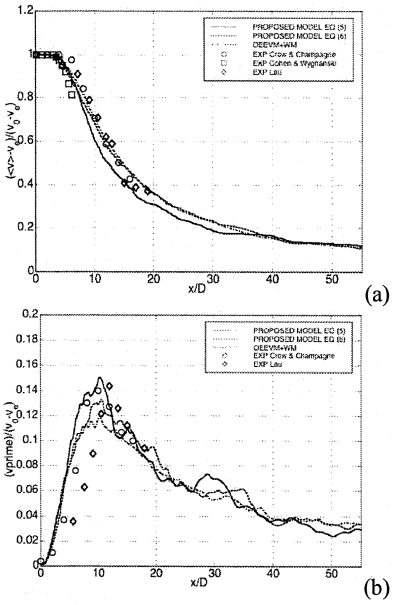

Figure 1. Round jet. Streamwise variation of the (a) streamwise velocity component and the (b) streamwise rms-velocity fluctuations on the medium grid.

In figure 2a and 2b we show radial profiles of $\langle \overline{v}_x \rangle$ and v_x^{rms} at x/D=4, 8, 16 and 32. All LES are in reasonable agreement with data, but with the proposed models showing somewhat better agreement with the $\langle \overline{v}_x \rangle$ data at x/D=4, 8 and 16. For v_x^{rms} we find that at x/D=4 both proposed models give better agreement with the data than the original LES model, with (5) giving the best agreement. At x/D=8 both proposed models again give better agreement with the data than the conventional LES model but now with (6) giving the best agreement. Note however that none of the LES are able to reproduce the strong dip in v_x^{rms} at x/D=4, whereas the corresponding dip at x/D=8 is reasonably well reproduced.

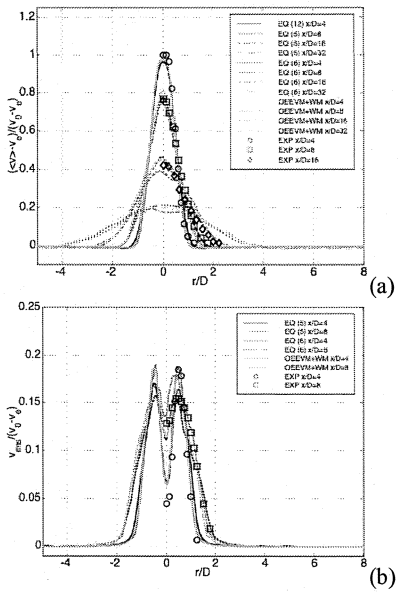

Figure 2. Round jet. Radial variation of the (a) streamwise velocity component and the (b) streamwise rms-velocity fluctuations at x/D=4, 8, 16 and 32 at the medium grid.

TURBULENT CHANNEL FLOW

The second test case is the fully developed turbulent channel flow. The channel is confined between two smooth parallel plates 2h apart, where h is the channel half-width. The flow is driven by a fixed mass flow in the streamwise ($\mathbf{e}_x$) direction. No-slip conditions are used in the cross-stream ($\mathbf{e}_y$) direction and periodic conditions are used in the spanwise ($\mathbf{e}_z$) direction. As initial conditions a parabolic $\overline{\mathbf{v}}$ distribution is used. For Re_τ=395 and 590, DNS data is available from Moser *et al.* (1999) and for Re_τ=1800 experimental data is available from Wei & Willmarth (1989). The physical channel size is 6h×2h×3h in the streamwise, cross-stream and spanwise directions, respectively. All LES calculations use 60^3 grids with uniform spacing in the streamwise and spanwise directions whereas the grid is gemetrically clustered in the wall-normal direction so that the spatial resolution varies between (Δx^+, Δy^+, Δz^+)=(40, 0.3, 20) and (180, 2, 90).

In figure 3a we compare the mean streamwise velocity $\langle \overline{v}_x \rangle$ (integrated over time, x and z) of the conventional LES model (1) using the DSMG and OEEVM+WM closure models, and the proposed models ((4) together with (5)-(6) and the wall model). At Re_τ=395 and 590 all LES are in good agreement with the DNS data across the channel, suggesting that at high enough resolution the details of the models are less important, and that the LES predictions approach that of DNS. At Re_τ=1800 differences between the models are starting to appear: Both the OEEVM and

DSMG models overpredict the velocity between $y^+\approx 50$ and 200, whereas the OEEVM+WM, and the proposed models, particularly that of (6) show good agreement with data. This implies that the wall model is important, and that this model is supported by the improved energy transfer of the modified Leonard term in the proposed models. In figure 3b we compare the predictions of the resolvable axial rms-velocity fluctuation $v_x^{rms+}=v_x^{rms}/u_\tau$, where now $v_x^{rms}=\langle(\overline{v}_x-\langle\overline{v}_x\rangle)^2\rangle^{1/2}$, with DNS and experimental results, Wei & Willmarth (1898). At Re_τ=395 all LES models show good agreement with the DNS data across the channel, however with a slight shift of the peak towards higher y^+. The DSMG models overpredict the peak value by a few percent whereas the OEEVM+WM is slightly more shifted towards higher y^+ values. At Re_τ=590 the scatter between the LES model predictions increases. Best agreement is obtained with the proposed models, in particular (6). The previously observed shift of the peak value towards higher y^+ values remains, and is somewhat more pronounced as is the overprediction of the peak value for the DSMG model. For Re_τ=1800 similar observations are made, but with more pronounced effects.

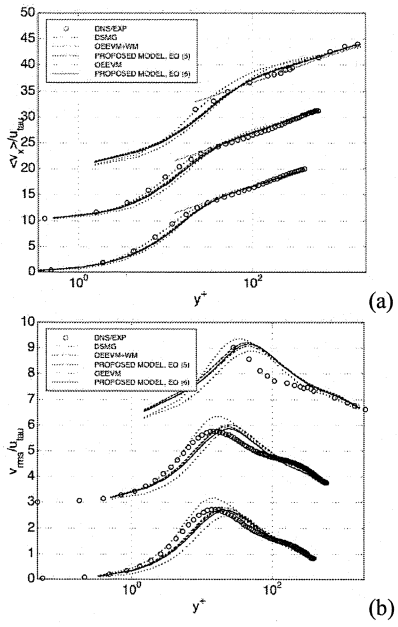

Figure 3. Fully developed turbulent channel flow. (a) Mean streamwise velocity profiles at Re_τ=395, 590 and 1800. The results for Re_τ=590 and 1800 are shifted 10 and 20 units, respectively, in the vertical direction. (b) Rms-velocity fluctuation profiles at Re_τ= 395, 590 and 1800.

FLOW PAST A CIRCULAR CYLINDER AT Re= 3900 AND Re=140,000

The third test case is that of the flow past a circular cylinder at Re_D=3900 and 140,000. Comparison is made between the traditional and proposed LES models and experimental data, Lourenco & Shih (1993), Ong & Wallace (1996) and Cantell & Coles (1983), at Re_D=3900, and 140, 000. In both cases, the computational domain is of rectangular form with a spanwise extent of 1.5πD. The cylinder is located 10D downstream of the inflow and 20D upstream of the outflow, and the vertical extent of the domain is 20D. The height of the first cell at the cylinder surface is $y^+\approx 10$ for both Re-numbers, resulting in grids with about $1.0\cdot10^6$ and $1.3\cdot10^6$ cells, respectively, with 48 cells in the spanwise direction. Conventional incompressible inflow and outflow boundary conditions are used together with periodic side condtions, slip conditions at the top and bottom and no-slip cylinder wall conditions. Figure 4a and 4b show perspective views of both cases, in terms of iso-surfaces of the second invariant of the velocity gradient, Q, identifying vortical regions. The influence of the Re-number on the wake is evident: at Re_D=3900 the wake is fairly wide but at Re_D=140,000 the width of the wake is much narrower since separation moves downstream with increasing Re_D. The wake consists of curved shear layers enclosing a region with vortices shed from alternate sides of the cylinder. The complex 3D vortex structures (spanwise quasi-2D vortices and longitudinal vortices) and the shear layers are clearly visible, although the complexity of the structures obscures the view.

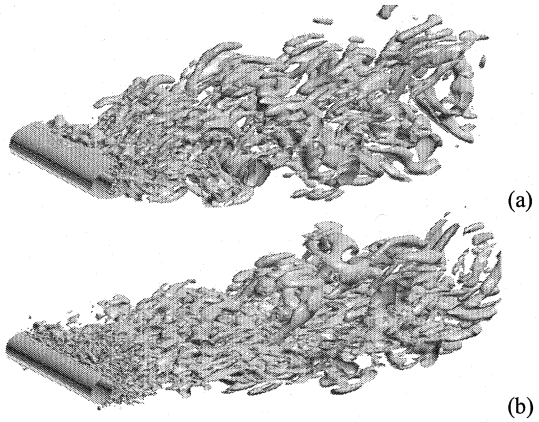

Figure 4. Flow past a circular cylinder. Perspective views of the flow at (a) Re_D=3900 and (b) Re_D=140,000 in terms of iso-surfaces of the second invariant of the velocity gradient tensor.

Figure 5a and 5b show the time-averaged streamwise velocity, $\langle\overline{v}_x\rangle/v_0$, for the Re_D=3900 and Re_D=140,000 cases, respectively, at different cross-sections. For Re_D= 3900 the comparison between LES and experimental data is satisfying. At x/D=1.06 and 2.02 very good agreement is found, whereas at x/D=1.54 all LES' underpredict $\langle\overline{v}_x\rangle$ with about 5%. Further downstream, at x/D=4.00, 7.00 and 10.0, good agreement is again obtained for all LES'. Virtually no difference can be found between the different LES, suggesting that at this resolution the influence of the closure model is small. For Re_D=140,000 we typically find larger differences among the predicted profiles, and between these and the experimental data. This is caused by the coarser resolution forcing the subgrid models to act in a wider range of scales. In particular, at x/D=1.00, 1.50 and 2.00 we find that the OEEVM+WM results in a more narrow wake as compared to the proposed models which show good agreement with the data. All models overpredict the peak reverse velocity with about 5% to 10%. Far downstream (x/D=4 and 7), good agreement between the predicted and measured velocity profiles is again obtained for all LES models.

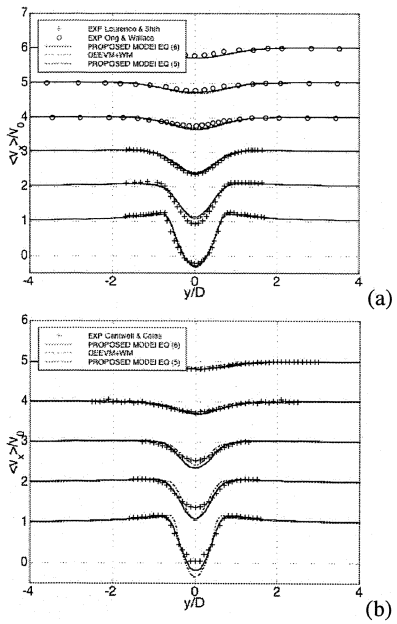

Figure 5. Flow past a circular cylinder. Time-averaged velocity at x/D=1.06, 1.54, 2.02, 4.0, 7.0 and 10.0 for (a) Re_D=3900 and at x/D=1.00, 1.50, 2.0, 4.0 and 7.00 for (b) Re_D=140,000.

FLOW PAST A PROLATE SPHEROID AT 10° AND 20° ANGLE OF ATTACK

The fourth case is that of the flow past a prolate spheroids at 10° and 20° angle-of-attack, Barber & Simpson (1991) and Chesnakas & Simpson (1996), in which a prolate spheroid (with a length of L=1.37 m) was mounted on a sting in a wind-tunnel of quadratic cross section. The free-stream velocity is v_0=46 m/s resulting in a body-length Re number of $Re_L = 4.0 \cdot 10^6$ and the angle-of attack was α=10° and 20°, Two grids with $0.8 \cdot 10^6$ cells ($y^+ \approx 30$) and $1.6 \cdot 10^6$ cells ($y^+ \approx 10$) are used. Conventional incompressible inflow and outflow boundary conditions are used together no-slip wall conditions. Following figure 6 the flow over a prolate spheroid at an incidence contains a rich gallery of complex 3D flow features. The flow separating from the leeward side of the body rolls up into a vortex on each side of the body and reattaches at the top-dead centre. This primary vortex is at higher α values accompanied by a secondary vortex that separates and reattaches higher up on the body. The complex interaction between vortices is strongly dependent on the angle of attack and the Re-number, and results in a highly skewed 3D-boundary layer. Boundary layer detachment is almost always accompanied by undesirable effects, such as loss of lift, increase in drag, and the amplification of unsteady effects including fluctuations in pressure. Prediction of 3D separation is hard and constitutes one of the main obstacles to more widespread use of CFD in analysis and design.

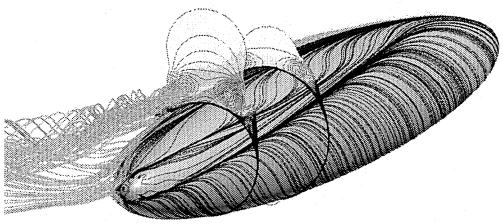

Figure 6. Flow around a prolate spheroid. Perspective view from the stern of the cross-flow separation and the longitudinal vortices around a 6:1 prolate spheroid at 20° angle-of-attack. The flow is represented by surface streamlines, streamlines released on the hull and contours of the instantaneous velocity magnitude at the cross-sections x/L=0.600 and x/L=0.772

Figure 7a and 7b show the static pressure coefficient C_P in the meridian plane and as a function of φ at x/L= 0.772, respectively. As seen in figure 7a, the agreement between LES and data for α=10° is very good. Along the wind-ward side at the stern there is some discrepancy, possibly due to the fact that the support sting used in the experiments is not included in the LES, see also Wikström *et al.* (2004). Compared to the distribution at α=10° the LES profiles at α=20° exhibit greater streamwise variation, corresponding to the stronger flow acceleration on the windward side and greater deceleration over the leeward side. In figure 7b, the agreement between LES and experimental data at α=10° is good with the exception of the sector 120°<φ<150°, that corresponds to the region beneath the primary vortex. For α=20°, C_P shows the existence of both a primary and a secondary separation on the body and the agreement between experimental data and LES is reasonable for the standard LES and slightly improved for the proposed models. Figure 7c and 7d shows the time-averaged boundary layer velocity profiles along rakes orthogonal to the hull at x/L=0.600, φ=90° and x/L=0.772, φ=60°, respectively. As shown by Wikström *et al.* (2004) the conventional LES model, using the OEEVM+WM,

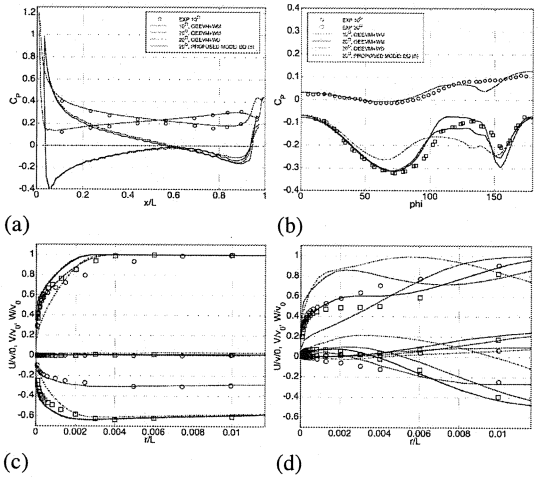

Figure 7. Flow around a prolate spheroid. Comparison of the static pressure coefficient, C_P, at (a) the meridian plane and (b) at x/L=0.772, and the normalized velocity (U, V, W) in the body surface coordinate system at (c) x/L=0.600 and φ=90° and (d) x/L=0.772 and φ=60°.

gives good agreement with the experimental data at three out of four rakes, with the fourth rake located at x/L= 0.772, φ=60°. From figures 7c and 7d it is clear that the proposed model (4) using the closure model (5) give equally good agreement with experimental data at x/L=

0.600 and φ=90°, as the conventional LES model, but considerably better agreement at x/L=0.772 and φ=60°. In fact very good agreement is also found between the proposed model and the data at x/L=0.600 and φ=60°, and x/L= 0.772 and φ=90°. The main reason for this improvement is that the predicted location of the primary vortex is in closer agreement with the measured location using the proposed model, the reason for which is believed to be the improved handling of the smallest resolved scales, and the associated interscale energy transfer, offered by including the modified Leonard term in the LES equations.

CONCLUDING REMARKS

From this mathematical investigation it is found that a modified Leonard stress tensor appears as an explicit term in the LES equations, together with a true subgrid stress term, composed of the modified cross and Reynolds stress tensors, that have to be modeled. This new formulation emphasizes the difference between RANS and LES, and reduces the modeling requirements for LES, and at the same time provides better correlations with DNS data in canonical flows. Furthermore, both the modified Leonard stress tensor, $\mathbf{L}$, and each for the remaining two parts of the subgrid stress tensor, the modified cross and Reynolds stress tensors, are individually frame-indifferent which simplifies the modeling and provides additional insight into the subgrid flow physics. Comparison of predictions from the proposed models and conventional LES models show that the former provide improved results in a range of flows.

ACKNOWLEDGEMENT

The authors wish to thank N. Wikström for providing all the prolate spheroid simulations.

REFERENCES

Barber K.M. & Simpson R.L.; 1991, "Mean Velocity and Turbulence Measurements of flow Around a 6:1 Prolate Spheroid", AIAA Paper 91-0255.

Bardina J., Ferziger J.H. & Reynolds W.C.; 1980, "Improved Subgrid Scale Models for Large Eddy Simulations", AIAA Paper No. 80-1357.

Cantwell B. & Coles D.; 1983, "An Experimental Study of Entrainment and Transport in the Turbulent Near Wake of a Circular Cylinder", *J. Fluid Mech.*, **136**, p 321.

Chesnakas C.J. & Simpson R.L.; 1996, "Measurements of Turbulence Structure in the Vicinity of a 3D Separation", *J. Fluids Eng.*, **118**, p 268.

Cohen, J. & Wygnanski I.; 1987, "The Evolution of Instabilities in the Axisymmetric Jet". Part 1. The Linear Growth of Disturbances Near the Nozzle., *J. Fluid Mech.*, **176**, p 191.

Crow S.C. & Champagne F.H.; 1971, "Orderly Structure in Jet Turbulence", *J. Fluid Mech.*, **48**, p 547.

Fureby C., Alin N., Wikström N., Menon S., Persson L., & Svanstedt N.; 2004, "On Large Eddy Simulations of High Re-number Wall Bounded Flows", *AIAA. J.*, **42**, p 457.

Fureby, C. & Tabor, G.; 1997, "Mathematical and Physical Constraints on Large Eddy Simulations", *J. Theoretical Fluid Dyn.*, **9**, p 85.

Germano M., Piomelli U., Moin P. & Cabot W.H.; 1991, "A Dynamic Sub Grid Scale Eddy Viscosity Model", *Phys. Fluids*, A **3**, p 1760.

Germano M.; 1986, "A Proposal for a Redefinition of the Turbulent Stresses in the Filtered Navier-Stokes Equations", *Phys. Fluids*, **29**, p 2323.

Hussein H.J.S., Capp S. & George W.K.; 1994, "Velocity Measurements in a High Reynolds-number, Momentum-conserving, Axisymmetric Turbulent Jet", *J. Fluid Mech.*, **258**, p 31.

Lau J.C., Morris P.J., Fisher M.J.; 1979, "Measurements in Subsonic and Supersonic Free Jets using a Laser Velocimeter", *J. Fluid Mech.*, **93**, p 1.

Lourenco L.M. & Shih C.; 1993, "Characteristics of the Plane Turbulent Near Wake of a Circular Cylinder, A Particle Image Velocimetry Study".

Moser R.D., Kim J. & Mansour N.N.; 1999, "Direct Numerical Simulation of Turbulent Channel Flow up to Re_τ=590", *Phys. Fluids*, **11**, p 943.

Ong J. & Wallace L.; 1996, "The Velocity Field of the Turbulent Very Near Wake of a Circular Cylinder", *Exp. in Fluids*, **20**, p 441.

Pope S.B.; 2000, "Turbulent Flows", Cambridge University Press.

Sagaut P.; 2001, "Large Eddy Simulation for Incompressible Flows", Springer Verlag, Heidelberg.

Schumann U.; 1975, "Subgrid Scale Model for Finite Difference Simulation of Turbulent Flows in Plane Channels and Annuli", *J. Comp. Phys.*, **18**, p 376.

Smagorinsky J.; 1963, "General Circulation Experiments with the Primitive Equations. I. The Basic Experiment", *Month. Wea. Rev.*, **91**, p 91.

Speziale C.G.; 1985, "Galilean Invariance of Sub Grid Scale Stress Models in the Large Eddy Simulation of Turbulence", *J. Fluid Mech.*, **156**, p 55.

Stolz S. & Adams N. A. & Kleiser L.; 2001, "An Approximate Deconvolution Model for Large-Eddy Simulation with application to Incompressible wall-bounded Flows", *Phys. Fluids*, **13**, p 997.

Van Cittert P.H.; 1931, "Zum Einfluss der Spaltbreite auf die Intensitätsverteilung in Spektrallinien II", *Z. Physik*, **69**, p 298.

Wei T. & Willmarth W.W.; 1989, "Reynolds Number Effects on the Structure of a Turbulent Channel Flow", *J. Fluid Mech.*, **204**, p 57.

Weller H.G., Tabor G., Jasak H. & Fureby C.; 1997, "A Tensorial Approach to CFD using Object Oriented Techniques", *Comp. in Physics*, **12**, p 629.

Wikström N., Svennberg U., Alin N. & Fureby C.; 2004, "LES of the Flow past an Inclined Prolate Spheroid", *J. Turbulence*, **5**, p 29.

Vreman B., Geurts B. & Kuerten H.; 1994, "Realizability Conditions for the Turbulent Stress Tensor in Large Eddy Simulation", *J. Fluid Mech.*, **278**, p 351.